Since January 2020 Elsevier has created a COVID-19 resource centre with free information in English and Mandarin on the novel coronavirus COVID-19. The COVID-19 resource centre is hosted on Elsevier Connect, the company's public news and information website.

BBA - Biomembranes 1861 (2019) 926–938

Contents lists available at ScienceDirect

BBA - Biomembranes

journal homepage: www.elsevier.com/locate/bbamem

Structure determination of UL49.5 transmembrane protein from bovine herpesvirus 1 by NMR spectroscopy and molecular dynamics

Natalia Karska[a], Małgorzata Graul[a], Emilia Sikorska[b], Igor Zhukov[c,d], Magdalena J. Ślusarz[b], Franciszek Kasprzykowski[b], Andrea D. Lipińska[a,1], Sylwia Rodziewicz-Motowidło[b,*,1]

[a] Intercollegiate Faculty of Biotechnology, University of Gdańsk and Medical University of Gdańsk, Abrahama 58, 80-307 Gdańsk, Poland
[b] Faculty of Chemistry, University of Gdańsk, Wita Stwosza 63, 80-308 Gdańsk, Poland
[c] Institute of Biochemistry and Biophysics, Polish Academy of Sciences, Pawińskiego 5a, 02-106 Warsaw, Poland
[d] NanoBioMedical Center, Adam Mickiewicz University, Umultowska 85, 61-614 Poznań, Poland

ARTICLE INFO

Keywords:
UL49.5 viral protein
BHV
TAP
NMR structure
Molecular dynamics
Molecular docking

ABSTRACT

The transporter associated with antigen processing (TAP) directly participates in the immune response as a key component of the cytosolic peptide to major histocompatibility complex (MHC) class I protein loading machinery. This makes TAP an important target for viruses avoiding recognition by CD8+ T lymphocytes. Its activity can be suppressed by the UL49.5 protein produced by bovine herpesvirus 1, although the mechanism of this inhibition has not been understood so far.

Therefore, the main goal of our study was to investigate the 3D structure of bovine herpesvirus 1 - encoded UL49.5 protein. The final structure of the inhibitor was established using circular dichroism (CD), 2D nuclear magnetic resonance (NMR), and molecular dynamics (MD) in membrane mimetic environments. In NMR studies, UL49.5 was represented by two fragments: the extracellular region (residues 1–35) and the transmembrane-intracellular fragment (residues 36–75), displaying various functions during viral invasion. After the empirical structure determination, a molecular docking procedure was used to predict the complex of UL49.5 with the TAP heterodimer.

Our results revealed that UL49.5 adopted a highly flexible membrane-proximal helical structure in the extracellular part. In the transmembrane region, we observed two short α-helices. Furthermore, the cytoplasmic part had an unordered structure. Finally, we propose three different orientations of UL49.5 in the complex with TAP. Our studies provide, for the first time, the experimental structural information on UL49.5 and structure-based insight in its mechanism of action which might be helpful in designing new drugs against viral infections.

1. Introduction

Herpesviruses (*Herpesviridae*) constitute one of the largest viral families with more than 100 representatives that have been identified thus far. They are one of the most prevalent pathogens that infect various organisms, with several widespread human pathogens, for example, herpes simplex virus 1 (HSV-1) and varicella zoster virus (VZV) [1]. Bovine herpesvirus 1 (BHV-1), related to VZV, is commonly known as an aggressive pathogen of cattle, causing infections of the respiratory and reproductive tracts. Consequently, BHV-1 and other veterinary herpesviruses lead to diseases that markedly affect agricultural incomes [2].

BHV-1 may affect the host's immune response by downregulation of the major histocompatibility complex class I (MHC I) molecules, followed by suppression of the normal activity of cytotoxic T lymphocytes [3]. This process is mainly controlled by the *UL49.5* gene product of BHV-1. UL49.5 is a small transmembrane protein composed of 75 amino acid residues [4]. During viral infection, this protein directly targets the transporter associated with antigen processing (TAP). In addition to BHV-1, several other related members of the *Varicellovirus*

Abbreviations: BHV, bovine herpesvirus; N.BHV, *N*-terminal fragment of UL49.5; TMC.BHV, transmembrane–*C*-terminal fragment of UL49.5; DPC, dodecylphosphocholine; CD, circular dichroism; MRME, mean residue molar ellipticity; NMR, nuclear magnetic resonance; NOE, nuclear Overhauser effect; NOESY, nuclear Overhauser effect spectroscopy; TAV, time averaged; MD, molecular dynamics; POPC, 1-palmitoyl-2-oleoyl-sn-glycero-3-phosphatidylcholine; TAP, transporter associated with antigen processing

* Corresponding author at: Faculty of Chemistry, University of Gdańsk, Wita Stwosza 63, 80-308 Gdańsk, Poland.
E-mail address: s.rodziewicz-motowidlo@ug.edu.pl (S. Rodziewicz-Motowidło).

[1] These authors jointly supervised the study.

https://doi.org/10.1016/j.bbamem.2019.02.005
Received 18 February 2018; Received in revised form 10 February 2019; Accepted 12 February 2019
Available online 14 February 2019

genus encode UL49.5 proteins with similar immune evasion activity [5]. TAP is a heterodimer consisting of two subunits: TAP1 and TAP2. In the host's immune system, the TAP heterodimer mediates the ATP-dependent transport of antigen-derived peptides from the cytoplasm to the endoplasmic reticulum (ER). Peptide transport by TAP is a bottleneck stage in the antigen presentation, thus it constitutes a perfect target for the UL49.5 protein [5]. Therefore, to design new vaccines or drugs against BHV-1, or use the virus as a vector in human therapy, it is very important to understand how the UL49.5 protein affects the TAP activity and triggers its degradation [6].

Each TAP subunit contains a transmembrane domain and a nucleotide binding domains (NBD) [7]. The NBDs are located on the cytosolic side of the ER membrane. The transmembrane domains of TAP1 and TAP2 are constructed of 10 and 9 helices, respectively, passing through the membrane [8]. Each transmembrane domain is composed of an *N*-terminal domain and a core domain. The *N*-terminal parts are responsible for binding tapasin and assembling the peptide loading complex. The core parts of TAP are responsible for peptide (substrate) binding and transport, in addition to the formation of the heterodimer structure [7].

The current mechanistic model for TAP describes three main conformations of the transporter: (1) an inward-open conformation, with the peptide binding site exposed to the cytoplasm and separated NBDs, (2) an intermediate pre-translocation conformation with the peptide binding-induced partial NBD closure [9], and (3) an outward-open conformation with a low-affinity peptide binding site exposed to the ER lumen and closely interacting NBDs [10,11]. UL49.5 interacts with the core transmembrane domain of TAP complex and blocks structural rearrangements required for the translocation of peptides into the ER lumen [11]. The conformational arrest of TAP causes sensitization of TAP proteins for proteasomal degradation. It has been demonstrated that the presence of both TAP1 and TAP2 is necessary for UL49.5 binding. UL49.5 has three biologically relevant domains: the ER lumen domain, the transmembrane region, and the *C*-terminal domain located on the cytosolic side [4].The membrane-anchored *N*-terminal UL49.5 domain seems to be crucial for the interaction and TAP inhibition. To understand the role of UL49.5 and both of the TAP subunits in the UL49.5–TAP complex, it is necessary to learn the 3D structure of UL49.5 [5]. Recently, the 3D structure of TAP bound to herpes simplex virus 1-encoded ICP47 protein was obtained using electron cryomicroscopy [12]. To the best of our knowledge, there is no information regarding the molecular structure of TAP in a complex with other viral transmembrane proteins, such as the US6 protein of human cytomegalovirus, the BNLF2a protein of the Epstein–Barr virus, the CPXV012 protein of the cowpox virus (reviewed in [13]), or any of the varicella virus-encoded UL49.5 [13].

The experimental determination of the UL49.5 structure is hampered by features typical of other transmembrane proteins: their hydrophobic properties, insolubility in an aqueous solution, difficulty to refold into their stable conformation, protein size, protein expression and purification, and difficulty to form diffraction-quality crystals [15]. In such difficult cases, the experimental results are very often supported by molecular modeling methods that are powerful tools for structural determination, the evaluation of protein–protein and protein–ligand interactions, and protein dynamics in a wide range of time scales. Therefore, in this study aimed at the understanding of the function of UL49.5, we determined the structure of the viral protein by using circular dichroism (CD), multidimensional NMR spectroscopy, and molecular dynamics (MD). For CD and NMR studies, the UL49.5 protein was divided into two peptides: (i) the ER lumen fragment (residues 1–35) and (ii) the transmembrane–intracellular fragment (residues 36–75), displaying various functions related to virus immune evasion. The CD spectra of these peptides were obtained in dodecylphosphocholine (DPC) micelles and in 1-palmitoyl-2-oleoyl-*sn*-glycero-3-phosphatidylcholine (POPC) vesicles, which were chosen as the mimetic models of the eukaryotic cell membrane [16–19]. The NMR spectra of these peptides were measured in micellar concentrations of DPC. Then, for both peptides, we used the NMR data as a set of restraints for an MD that generated 3D structures of peptides in DPC micelles. We performed MD simulations in an explicit water/DPC micelle as the biological membrane environment. On the basis of the structure of peptide fragments 1–35 and 36–75, we built the full structure of the UL49.5 protein and performed MD studies in the POPC bilayer. Finally, the performed structure of the UL49.5 was used as a ligand in the molecular docking procedure with TAP.

2. Materials and methods

2.1. Peptide synthesis and purification

All the peptides were synthesized using the standard solid-phase synthesis technique (Millipore 9050 Plus PepSynthesizer, Millipore Corporation, Burlington, VT, USA) at TentaGel R RAM resin (capacity 0.2 mmol/g, Rapp Polymere GmbH. Germany) according to the Fmoc-chemistry strategy [20,21]. The protected amino acids and the other chemicals were purchased from NovaBiochem (Nottingham, UK) or Sigma-Aldrich (Poznan, Poland). The peptides were cleaved from the resin by using a mixture of trifluoroacetic acid, triisopropylsilane, phenol, and water (0.8:0.5:0.5:0.2) at room temperature for 3 h with gentle shaking. After the filtration of the exhausted resin, the solution was concentrated in vacuum, and the resin was triturated with Et_2O. The precipitate peptide was centrifuged for 15 min at 4000 rpm, followed by the decantation of the ether phase from the crude peptide (the process was repeated three times).

To avoid problems related to dimerization by the oxidation of the sulfhydryl group of cysteine and/or the formation of diastereoisomeric sulfoxides by the oxidation of the methionine thioether moiety, methionine and cysteine were replaced with isosteric norleucine (Nle) and (*S*)-2-aminobutyric acid (Abu), respectively.

Synthetic peptides (an *N*-terminal fragment of UL49.5 (N.BHV) and *C*-terminal fragment of UL49.5 (C.BHV)) were purified using reversed-phase high-performance liquid chromatography (RP-HPLC) on a system consisting of two Knauer K1001 pumps and a UV–vis detector-equipped Gilson fraction collector. N.BHV and C.BHV were purified using a 10 mm × 250 mm Kromasil C-8 column (particle diameter: 5 μm, pore size: 300 Å). N.BHV was purified using linear gradients of the acetonitrile–water mixture (containing 0.1 M TEAP, pH = 3) as an eluent. C.BHV was purified using linear gradients of the acetonitrile–water mixture (containing 0.1% (v/v) TFA) as an eluent. The purification of a transmembrane-*C*-terminal fragment of UL49.5 (TMC.BHV) peptide was performed on a semi-preparative 10 × 250 mm Kromasil C-4 column (particle diameter: 5 μm, pore size: 300 Å), using linear gradients of methanol–water mixture (containing 0.1% (v/v) TFA) as an eluent. The flow rate was 5 mL/min. TMC.BHV was detected at the wavelength of 223 nm. A transmembrane fragment of UL49.5 (TM.BHV) was purified on a Sephadex LH20 column with methanol. The purity of all the peptides was higher than 98% as estimated with RP-HPLC.

The identity of peptides was confirmed by matrix-assisted laser desorption ionization-time of flight (MALDI-TOF MS; see Table 1S in Supplementary materials) and electrospray ionization mass spectrometry (ESI-MS). The MALDI-TOF MS spectra were acquired on the Bruker Biflex III MALDI-TOF spectrometer by using an ultraviolet laser source (nitrogen, 337 nm); α-cyano-4-hydroxycinnamic acid was used as the matrix. The ESI-MS spectra were recorded on a Shimadzu IT-TOF mass spectrometer.

2.2. CD spectropolarimetry

CD studies were performed in DPC micelles (25 mM and/or 100 mM, POCh, Poland) in water (pH = 7.0) or PBS (pH = 7.4) and POPC liposomes (0.1, 0.3, and 0.5 mM) in water. The CD spectra of

TMC.BHV in PBS were not recorded because of its insolubility under these conditions. The peptide solutions in the DPC micelles were prepared according to the standard procedures [19,22]. POPC (Avanti; Alabaster, AL) was dissolved in chloroform, which was evaporated by blowing a slow stream of nitrogen gas and then dried under vacuum conditions. Afterward, the lipid thin film was hydrated with pure water and the sample was mixed thoroughly at 40 °C for 2 h to produce MLVs suspension. Finally, MLVs suspension was sonicated at 40 °C to prepare SUV liposomes and fully transparent solution.

The CD spectra were recorded for 0.15 mg/mL peptides in the range of 185–260 nm with the Jasco J-815 spectropolarimeter (Jasco, Easton, USA). For each peptide, the CD spectra were recorded three times, at 30 °C. using a 1-mm cell and showed as the mean residue molar ellipticity (MRME, degree × cm^2 × $dmol^{-1}$) against the wavelength λ (nm). The content of the helix structure in each peptide was calculated based on the intensity of the band at 222 nm, using the formula from the literature [23].

2.3. NMR spectroscopy

NMR experiments were performed using 100 mM DPC-d_{38} (POCH S.A. Poland) in water (90%:10% H_2O:D_2O). The peptide concentration was 4.8 mM (N.BHV) and 2.7 mM (TMC.BHV). The DPC-d_{38}:peptide ratio was kept approximately to 40:1, and the pH was adjusted to 5.0 [24]. To improve the micelle formation and the binding of the synthesized peptide to the DPC micelle as well as the homogeneity of this complex, each sample was sonicated for 10 min at room temperature. All NMR datasets were acquired at 303 K on a Bruker Avance III NMR System 700 NMR spectrometer (700 MHz 1 H. 16.4 T) or on an Agilent DDR2 800 MHz NMR spectrometer (800 MHz. 1 H. 18.8 T). Both spectrometers were equipped with four channels, z-gradient unit, QCI (^{1}H, ^{13}C, ^{31}P, and ^{15}N), or ^{1}H/^{13}C/^{15}N triple probe head with inverse detection. Sequential backbone resonance assignments were obtained according to a standard procedure based on an analysis of the 2D NMR spectra [25]. In our study, the analyzed NMR datasets included the following: (i) double-quantum filtered correlation spectroscopy (DQF-COSY) [26]; (ii) total chemical shift correlation spectroscopy (TOCSY) [27] acquired at a mixing time of 80 ms; (iii) nuclear Overhauser effect spectroscopy (NOESY) [28] recorded with the mixing times of 100, 200, and 400 ms; and (iv) the rotating-frame Overhauser enhancement spectroscopy (ROESY) [29] collected with the mixing times of 150 and 200 ms. The data were recorded as 1024 × 512 complex data points processed with double zero filling and a cosine squared sinebell weighting function along all the dimensions. The excitation sculpting the double pulse field gradient spin echo (DPFGSE) pulse block was used to suppress the signal of the water molecules in all the acquired data [30], which resulted in perfect suppression and a linear baseline. Homonuclear experimental datasets were additionally supplemented with heteronuclear 2D ^{1}H−^{13}C HSQC (tuned independently to the aliphatic and aromatic regions) as well as the 2D ^{1}H−^{15}N HSQC NMR experiments performed on the basis of natural abundance of the ^{13}C and ^{15}N, nuclei. All the NMR experiments were referenced indirectly with an external reference, that is, sodium 2.2-dimethyl-2-silapentane-5-sulfonate (DSS) with the Ξ = 0.251449530 and 0.101329118 coefficients for ^{13}C and ^{15}N respectively [31,32]. The acquired datasets were processed with the NMRPipe software [33] and analyzed with the Sparky [34] program.

2.4. Structural calculation of peptides

The interproton distances were calculated on the basis of the NOE intensities extracted from the NOESY spectra at a mixing time of 200 ms. Here, 485 and 343 distance restraints were provided for N.BHV and TMC.BHV, respectively. The initial structures of the N.BHV and TMC.BHV peptides were calculated by the simulated annealing algorithm, which included 10,000 steps of MD in the torsion angle space (CYANA software) [35]. As a result the calculation protocol initialized with 200 structures created randomly chosen torsion angles.

2.5. Construction of peptides in DPC micelle and MD simulations

The starting coordinates of the DPC micelle–water system were taken from simulations conducted by Tieleman *et al.* [36]. A single molecule of DPC was constructed on the basis of previously published parameters [37,38]. The pre-built hydrated DPC micelle consisted of 65 DPC monomers and 6305 water molecules. The DPC topology was adapted to AMBER [39,40]. Then each peptide was placed in a simulation box with its center of mass coinciding with the DPC micelle. The 3D structures of the N.BHV and TMC.BHV peptides evaluated with CYANA were used as the starting structure in the MD calculations of the DPC micelle. The side chains of lysine and arginine were protonated, and chloride ions were used to neutralize the total charge of the entire system. The entire system was subjected to energy minimization (steepest descent method). To eliminate the initial adverse interactions between the peptide and the micelle core and to prevent the penetration of water molecules during equilibration, for the first 20,000 steps of minimization, the peptide and the water were kept under weak harmonic constraints with a force constant of 10 and 5 kcal/mol, respectively. Then, each system was subjected to NTP MD for 20 ns at 305 K at time steps of 2 fs. During the MD stimulation, a non-bonded cutoff of 9 Å was chosen. The MD studies for the DPC micelle/water/peptide complex were performed with the AMBER software [39] by using a protocol including time-averaged NMR restraints (TAV) derived from NMR spectroscopy with the force constant for interproton connectivities equal to 50 kcal/(mol × $Å^2$). No torsion angle restraints were used in the calculations. The geometry of the peptide groups was kept all *trans* with the force constant of f = 50 kcal/mol × rad^2, according to the NMR data. The coordinates were collected every 2000 steps. The 20 structures obtained in the last step of the MD simulation were considered for further analysis. All the figures were evaluated by using the MOLMOL [41] or PyMOL [42] program.

The structures of nonstandard amino acid residues (Nle and Abu) were built based on the bond lengths, valence and torsion angles for the standard residues in the AMBER library [39,40]. The point charges were optimized by fitting them to the *ab initio* molecular electrostatic potential (GAMESS'04, *ab initio* molecular electronic structure program, [43]) for three different conformations, followed by the consecutive averaging of the charge over all of the conformations, as recommended by the RESP protocol [44].

During the MD simulations, both peptides diffused from the hydrophobic core of the DPC micelle to an interface, to adopt a more energetically favorable conformation. The interactions between the peptide and the micelle were analyzed by the radial distribution function (RDF) for all the amino acid residues for both peptides using the Ptraj program from the AMBER 11.0 package [39,40]. The geometric analyses were performed using the MolProbity [45]. The hydrogen bonds were analyzed using the MOLMOL program [41]. Salt bridges were evaluated using the ESBRI software [46].

2.6. MD simulations of UL49.5 in POPC membrane model

The 3D model of UL49.5 was created according to the results obtained from the MD calculations with the NMR restraints. The N.BHV and TMC.BHV peptides were combined using PyMOL and the standard AMBER tools [40]. Next, the achieved protein was placed in the fully hydrated POPC membrane model [17,47]. The periodic box contained 50 POPC lipid molecules, more than 2500 water molecules, and 4 Cl^- counter ions. The system was initially minimized and subsequently submitted to 90 ns of MD simulations in the AMBER program, using the particle-mesh Ewald (PME) electrostatic summation [39,48]. For the first 40 ns of the MD, the flat-bottom soft harmonic-wall restraints were imposed onto the ϕ and ψ angles (with the force constant f = 40 kcal/

mol × rad^2) of the amino acid residues. For the next 50 ns of the simulation, free MD without any restraints was performed. The final protein structure was minimized. The trajectories were analyzed using the Ptraj module from the AMBER package [39]. The distance between the transmembrane α-helix (V40-M46) and the α-helix (V49-F58) was measured for the mass centers of the V40 and F58 amino acid residues by using a Ptraj module. Similarly, in the Ptraj module, the diffusion of the αC atoms as a mean square displacement was calculated. The chart was drawn in Gnuplot [48].

2.7. Molecular docking of UL49.5 to TAP

The molecular docking of UL49.5 to TAP was conducted to obtain the UL49.5/TAP protein complex. The available 3D structure of TAP heterodimer was used (PDB code: 5u1d, [49]. In the next step, the substrate (H_2N-R^{1}RYQK5STEL^9-$CONH_2$ peptide [5,7]) was docked to the UL49.5/TAP complex. Docking was performed using the ClusPro v.1.0 [50,52] program. The molecular docking procedure used the final UL49.5 structure received after MD. The substrate of TAP [5], with the amino acid sequence H_2N-R^{1}RYQK5STEL^9-$CONH_2$, was built using PyMOL [42]. This peptide at the beginning possessed a stretched conformation, and then, its structure was optimized using the minimizing energy *in vacuum* with the AMBER program [39]. During the molecular docking of UL49.5 to TAP or the substrate (H_2N-R^{1}RYQK5STEL^9-$CONH_2$ peptide) to the UL49.5/TAP complex, a blind docking method was used.

3. Results and discussion

3.1. Design of peptides for CD and NMR studies

The ER-resident UL49.5 consists of 75 amino acid residues, and thus far, its structure has not been established because of its strong tendency to form aggregates. Before this work, an attempt to receive UL49.5 aa17–96 fused to GST as a carrier protein was made to express it in the bacterial system. We hoped to obtain a soluble protein, similar to the viral membrane proteins for HIV gp41 (a fragment 677–716) and the Ebola virus (45-aa long MPER/TM fragment) viral fusion proteins [53,54]. However, recombinant UL49.5 was fully insoluble, forming inclusion bodies, and we were unsuccessful in its refolding after the solubilization of the inclusion bodies by using the descending gradient of urea. This has discouraged us from performing purification under denaturing conditions. The tagging of the UL49.5 protein has thus far affected the UL49.5 activity (unpublished data); hence we did not proceed with these experiments, even if the tag could be removed by the protease cleavage. Therefore, we decided to synthesize the UL49.5 fragments chemically. UL49.5 was divided into three protein fragments on the basis of its predicted structure [55]. The *N*-terminal fragment (N.BHV) and the *C*-terminal fragment (C.BHV) of UL49.5 are located outside the membrane, while the middle transmembrane one (TM.BHV) buried inside the hydrophobic core of the cellular of virus envelope membranes (Table 1) [55].

During the synthesis, we observed that all of the synthesized peptides possessed the expected molecular weight (Table 1S), although the TM.BHV peptide was insoluble in any of the applied solutions (acetic acid, dimethyl sulfoxide, 6 M urea, water, and methanol). Therefore, instead of the TM.BHV and C.BHV peptides, another peptide (TMC.BHV) was prepared, which combined two UL49.5 fragments: the transmembrane and *C*-terminal (Table 1).

Table 1
Sequence of UL49.5 peptide fragments.

Symbol	Sequence of the native protein peptide fragments
N.BHV	R^{1}DPLLDAMRREGAMDFWSAGCYARGVPLSEPPQAL^{35}
TM.BHV	V^{36}VFYVALTAVMVAVALYAYGLCF^{58}
C.BHV	R^{59}LMGASGPNKKESRGRG^{75}
TMC.BHV	V^{36}VFYVALTAVMVAVALYAYGLCFRLMGASGPNKKESRGRG^{75}

To overcome the problems related to the dimerization of the sulfhydryl groups of cysteine and/or the formation of diastereoisomeric sulfoxides *via* the oxidation of the methionine thioether moiety, methionine and cysteine were replaced with isosteric norleucine (Nle) [56–58] and (*S*)-2-aminobutyric acid (Abu) [56] in the synthetic peptides, respectively. In addition, cysteine and methionine could negatively influence the cleavage of the protecting groups during the chemical synthesis and the subsequent peptide purification. Thus, the thioether functional group of methionine is susceptible to oxidation, creating two diastereomeric sulfoxides with sulfone. Note that the methionine and cysteine residues have a very similar structure (the volume of the amino acid atoms) and the distribution of partial charges to Nle and Abu, respectively.

Additionally, our unpublished results indicate that the mutation of M46 in the UL49.5 protein revealed no significantly effects on the protein activity (data not shown). Since then, we assumed that the potential Nle-evoked changes in the protein structure might play an insignificant role in the further 3D structure. In contrast, the C21 residue has an important function in the UL49.5 bonding to the viral gM protein [54,59] and not to TAP. In addition, the C57 residue did not affect the biological activity of the protein at all [54,59].

3.2. CD measurements of N.BHV and TMC.BHV-1 reveal unstructured conformation in aqueous and α-helical conformation in DPC and POPC environments

The CD spectra of N.BHV in water or in PBS exhibited a characteristic negative band at 199 nm, indicating mainly an unordered structure (Fig. 1A). The CD spectra of TMC.BHV in water exhibited a characteristic negative band at 215 nm, which is characteristic for beta structure. The peptide has a predominantly beta conformation in water, which may be related to some aggregation (Fig. 1B). The CD spectrum of TMC.BHV in PBS was not recorded because of its insolubility. The addition of DPC or POPC considerably changed the CD spectra of both peptides (Fig. 1A–D). The membrane mimetic environment (DPC or POPC) induced the α-helical structure observed as two negative values of a molar ellipticity observed around 205 and 222 nm and positive values around 192 nm. With N.BHV, the intensity of the 206 nm band increased with an increase in the DPC or POPC concentration (Fig. 1A and C). In case of TMC.BHV, the changes in the DPC or POPC concentrations were insignificant for its CD spectrum (Fig. 1B and D).

The quantitative CD spectral analysis for both peptides show, that at the 100 mM concentration of DPC or at the 0.1 mM concentration of POPC, the CD spectra of both peptides showed the maximum α-helical content. The quantitative CD spectral analysis for peptides dissolved in 100 mM DPC indicates that the content of the helical structure was 17% and 26% for N.BHV and TMC.BHV, respectively (Fig. 1S A and B). The content of the helical structure in 0.1 mM POPC was only 12% for N.BHV and 44% for TMC.BHV (Fig. 1S A and B). The obtained results showed that for N.BHV in POPC there is less content of helix than in DPC, whereas for TMC.BHV in POPC there is more helix content than in DPC.

The mean residue molar ellipticity (MRME) values observed in the CD spectra of N.BHV were found to be lower for the studies in water than in the PBS solution. Also the content of the helical structure of N.BHV depended on the concentration of the surfactant used (Fig. 1S A). Thus, we assumed that the conformation of N.BHV was very sensitive to the ionic strength and to the surfactant concentration. This might indicate that N.BHV was located on the surface of the DPC micelle or POPC membrane.

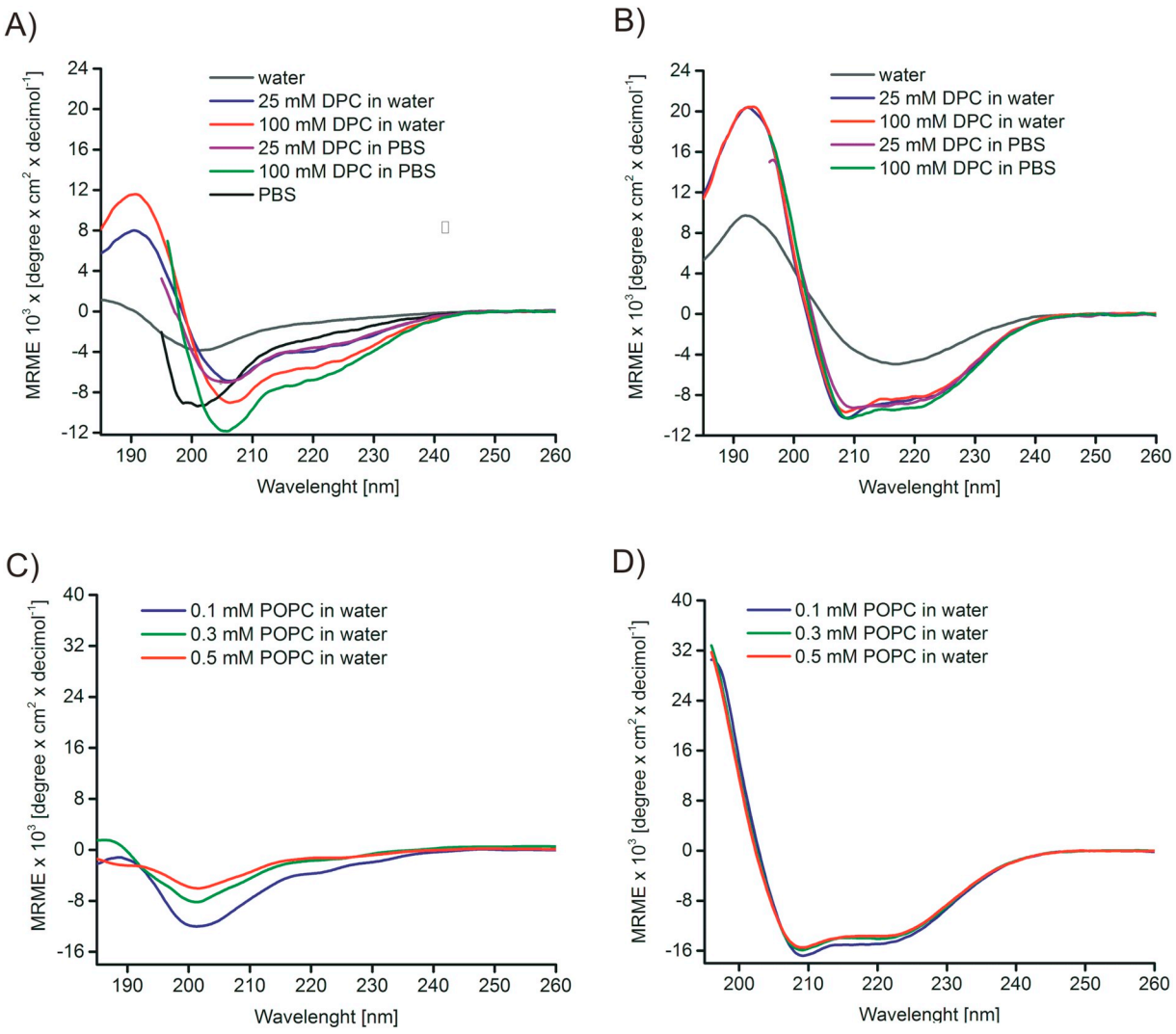

Fig. 1. CD spectra of (A) N.BHV and (B) TMC.BHV peptides in DPC micelles in water or in PBS at pH 7.4. CD spectra of TMC.BHV in PBS were not collected because of its insolubility under these conditions. CD spectra of (C) N.BHV and (D) TMC.BHV peptides in POPC vesicles in water. All spectra were measured at 30 °C in 1 mm optical path length.

3.3. Assignment of resonances in N.BHV peptide in DPC-d_{38} micelle environment

The assignment of the ^{1}H resonances was performed for N.BHV peptide on the basis of the 2D homonuclear TOCSY (Fig. 2S) and NOESY (Fig. 3S) spectra in 100 mM DPC-d_{38} micelle environment (Table 2S, BRMB code: 27728). The sequential assignments were achieved by using the 2D homonuclear NOESY spectra. In the case of N.BHV, two distinct sets of proton resonances in the membrane-proximal part of the peptide (residues L28, S29, and A34) were found (Fig. 2S). The appearance of two conformers might be the result of the presence of the two proline residues at positions 31 and 32, and consequently, the cis/trans isomerization of the peptide bonds. For the peptide bonds in which the proline residues were involved, the following NOE signals were observed: αH^{D2}-δH^{P3}, αH^{V26}-δH^{P27}, αH^{E30}-δH^{P31}, and δH^{P31}-αH^{P32}. This observation together with the lack of signals characteristic for the *cis* peptide bond geometry indicated the all *trans* bond geometry for the major conformation of N.BHV. The chemical shifts of the corresponding protons in the two conformers of N.BHV were very similar, and the differences were no greater than 0.25 ppm. The NOESY (Fig. 3S) spectrum of N.BHV showed 485 NOE connectives including 109 intraresidue, 181 sequential, and 195 medium-range signals. The medium and long-range NOE interactions occurred along the entire peptide's main chain, indicating a stable secondary structure. The observed NOE effects of αH-$NH_{(i,i+2)}$, αH-$NH_{(i,i+3)}$, αH-$\beta H_{(i,i+3)}$, and αH-$NH_{(i,i+4)}$ showed the existence of the regular α-helical structure in the A7-G20 fragment of N.BHV (Fig. 2A).

3.4. Assignment of resonances in TMC.BHV peptide in DPC-d_{38} micelle environment

The ^{1}H resonances were assigned for TMC.BHV peptide on the basis of the 2D homonuclear TOCSY (Fig. 4S) and NOESY (Fig. 5S) spectra in the 100 mM DPC-d_{38} micelle environment (Table 3S, BRMB code: 27730). In the case of TMC.BHV, one set of protons was predominantly found in the DPC micelle environment, except for the two residues N67 and S71 (Fig. 4S). The existence of the P66 residue might explain the two distinct sets of the proton resonances in the 2D NMR spectra. For the peptide bond with P66 residue, the NOE signal of αH^{G65}-δH^{P66}, confirmed the presence of a *trans* peptide bond geometry. In 100 mM DPC-d_{38}, the NOESY (Fig. 5S) spectrum of TMC.BHV showed 344 NOE connectives including 2 long-range, 125 intraresidue, 133 sequential, and 84 medium-range effect. The NOE effects of αH-$NH_{(i,i+3)}$, αH-$\beta H_{(i,i+3)}$, and αH-$NH_{(i,i+4)}$ showed an α-helical structure in the V37-V45 and V48-L60 regions of TMC.BHV (Fig. 2B). The characteristic NOE interactions αH^{V47HA}-HN^{V49}, HN^{A48}-HN^{V49}, αH^{A48}- HN^{V49}, and

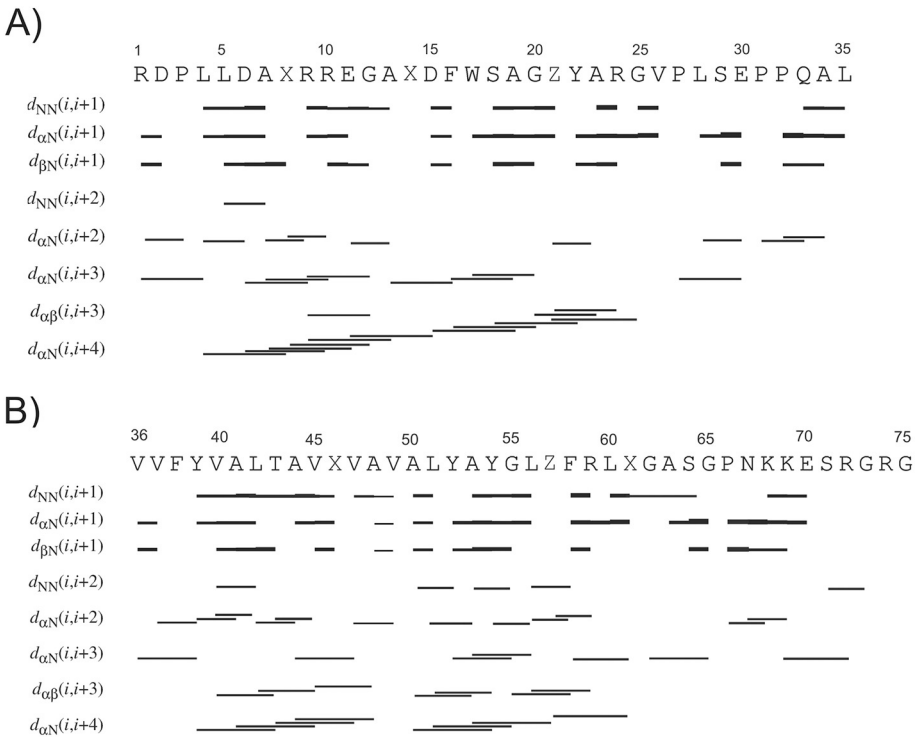

Fig. 2. Summary of inter- and intra-residue NOEs between backbone NH, αH, and βH for (A) N.BHV and (B) TMC.BHV peptides, measured in NOESY spectrum (200 ms) in 100 mM DPC-d_{38} H_2O/D_2O at 30 °C. X and Z correspond to norleucine and aminobutyric acid, respectively.

βH^{A48}-HNV^{49} indicated the presence of the beta-turn located at positions 47 and 48 (see Figs. 2B and 5S). During the integration of NOE signals was raised the level of integration in the NOESY spectrum. Therefore, we lost the less intense NOE signals, which is the reason for the lack of NOE signal in some places in Fig. 2. In addition the lack of certain NOEs in helices in these helical regions is due to the fact that the signals were strongly overlapping and therefore were not integrated.

3.5. Analysis of 3D structure of N.BHV peptide in DPC micelle

N.BHV (PDB code: 6QAN) adopted a right-handed α-helical structure in its middle region (A7-G20) with unordered *N*-(R1-L5) and *C*-(Abu21-L35) termini (Fig. 3A). Four salt bridges were formed in the peptide's structure, the first between the R1–E11 residues, the second between the D6–R9, next between the D6–R10, and last between R24–E30 residues. In the α-helical region, the RMSD value for the backbone atoms was 0.18 Å, while that for heavy atoms was 0.31 Å. This indicated rigid and stable the α-helical structure. The *C*-terminal fragment of N.BHV adopted a disordered structure with a β-turn. Such a turn was formed in the V26-S29 region (VPLS) and stabilized by the hydrogen bond between the V26 carbonyl oxygen and the S29 amide proton. The second turn was formed in the E30-Q33 region (EPPQ) and stabilized by the hydrogen bond between the E30 carbonyl oxygen and the Q33 amide proton (Fig. 3A).

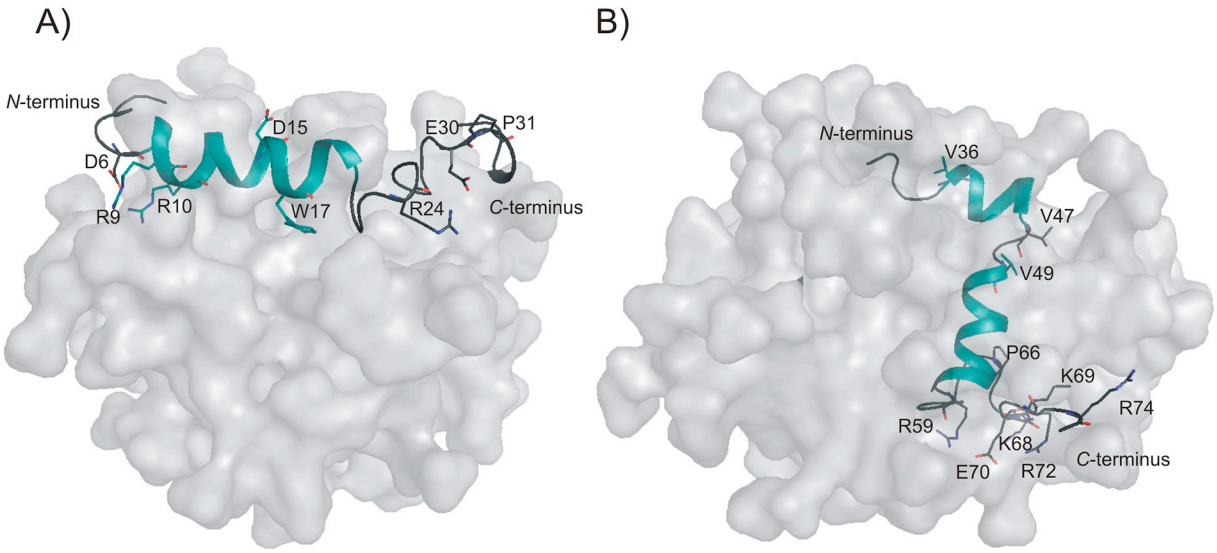

Fig. 3. High-resolution 3D structures of (A) N.BHV and (B) TMC.BHV in DPC micelle obtained after 20 ns of molecular dynamics simulations using TAV procedure in AMBER program. DPC micelle is presented as surface. Oxygen atoms are represented in red, and nitrogen atoms are represented in dark blue.

N.BHV moved out of the DPC micelle core completely after approximately 12 ns of MD simulations. Thereafter, it remained bound to the interface for a further subsequent steps of MD simulations. Its RDF analysis showed that under infectious ongoing processes, the N.BHV fragments D2-P3, L5-Nle8, A23-G25, and S29-L35 (with the exception of Q33), and the A19 residues were exposed to an aqueous environment. The fragments R9-G12, D15-F16, V26-P27 and R1, L4, S18, Q33 residues were located at the micellar surface and mostly interacted with the hydrophilic heads of the surfactants. The residues (moieties) W17, L28 and A13-Nle14, G20-Y22 of N.BHV were immersed in the hydrophobic micellar core of the DPC micelle (Fig. 6*S*).

3.6. Analysis of 3D structure of TMC.BHV peptide in DPC micelle

TMC.BHV (PDB code: 6QBJ) formed two α-helical fragments in the V40-Nle46 and V49-F58 (transmembrane helices 1 and 2) regions (Fig. 3B). In the hydrophobic part of the micelle, the transmembrane helices 1 and 2 were connected by β-turn located at positions 47 and 48 (Fig. 3B). The interhelical angle between both the transmembrane helices was approximately 90°. In the α-helical region, the RMSD value of the backbone atoms was 0.12 Å, while that for heavy atoms was 0,25 Å. The *C*-terminal fragment of the peptide was mainly unstructured, with tendency to a wide bent formation in the Nle61-P66 region. This structure was stabilized by the salt bridge between the residues R59 and E70 (Fig. 3B). The *C*-terminus of TMC.BHV moved out of the DPC micelle completely after approximately 6 ns of MD. In contrast, the remaining part of TMC.BHV stayed in the hydrophobic micellar core until the end of the dynamic study. The RDF analysis showed that the V36-F38, A44-V45, S64-K68, E70-S71 fragment V40 and V47 residues were exposed to water (Fig. 7S), while the L42-T43, A48-A63 (with the exception of R59) fragment and Y39 residue were located inside the hydrophobic micellar core. The positively charged centers of the K68, R72 and R74 side chains showed a tendency to be associated with the phosphate groups of the DPC molecules.

The Ramachandran plots, calculated for both N.BHV and TMC.BHV, showed that most of the residues were located in the allowed regions of the plot (Fig. 8S, Table 4S). The Ramachandran plot was calculated for structures from the last 20 steps of molecular dynamics.

3.7. Structure and dynamics of UL49.5 in POPC membrane

The model of UL49.5 protein was constructed by connecting the *C*-terminus of N.BHV and the *N*-terminus of TMC.BHV, while maintaining the experimental structure of both the peptides. Both fragments were joined using the PyMOL program [42] and the standard tools of the AMBER program [40]. In the construct, the Abu and Nle residues existing in N.BHV and TMC.BHV were replaced by the Cys and Met residues, respectively, occurring naturally in the sequence of native UL49.5, respectively. In the next step, the protein was positioned in a fully hydrated bilayer of POPC (biological membrane model), followed by the minimization and MD simulations. During the first 40 ns of MD, all the helical structures were frozen according to the NMR data, while the rest of the protein fragments could move freely. For the next 50 ns, all the restraints were removed.

At the 0 ns time point, the *N*-terminal helix (helix 1) was partly submerged in the membrane (Fig. 4). The S18-V37 and R59-G75 regions were located on the polar side of the POPC membrane, while the rest of the UL49.5 protein was placed in the POPC hydrophobic core. Both transmembrane helices (helix 2 and 3) were oriented at an angle of *ca.* 90° to each other (Fig. 4, 0 ns). After ~30 ns of the MD simulation (Fig. 4, 30 ns), helix 1 emerged from the POPC membrane. When the NMR restraints were removed, helix 1 unfolded slightly in its middle part (Fig. 4, 90 ns) but maintained its overall helical character. Helix 1 could move freely in all the directions above the membrane's surface (Fig. 4) during MD. These free movements were facilitated by the presence of the C21-Y39 unstructured protein fragment. During the MD simulations, both transmembrane helices were displaced and their *N*-ends were separated further than in the starting structure, however, their length remained the same. The interhelical angle between both transmembrane helices was approximately 110° in the final structure. The *C*-terminal fragment of UL49.5 remained in the charged part of the POPC membrane during the entire MD simulation.

To describe the degree of mobility of a given amino acid residue during the MD calculations, the values of the root-mean-square fluctuations (RMSFs) were calculated. By analyzing the changes during the MD simulations, we found that all the RMSF values increased slightly after the first 40 ns of the MD simulation (Fig. 5). After this time, the RMSF did not change significantly until the end of simulation (90 ns). On the basis of the RMSF values, UL49.5 was found to be characterized by significant mobility in the *N*-terminal region (residues 1–15), including helix 1 (Fig. 5). The rest of the protein exhibited considerably lower mobility with respect to the *N*-terminus.

In general, UL49.5 adopted a stable α-helical conformation when inserted into the POPC membrane during 90 ns of the MD simulation. The final structure of UL49.5 (Fig. 6A) in the POPC membrane consisted of three α-helical regions. The first α-helix (helix 1) was located in the N-terminal fragment (D2-G20, helix 1) (ER lumen domain). The next two helical fragments were formed in the V40-M46 (helix 2) and V49-F58 (helix 3) regions. Most of the hydrogen bonds and salt bridges observed in N.BHV and TMC.BHV studied separately were preserved in the structure of the construct of the UL49.5 protein located in the POPC membrane. The characteristic salt bridges existing in the N-terminus of UL49.5 were clustered in its very beginning, namely residues R^{1}DPLL-DAMRRE^{11}, where three positively and three negatively charged amino acids are present. Three salt bridges were observed between R^{9}-D^{2}, R^{9}/R^{10}-D^{6}, and R^{10}-E^{11}. A fourth salt bridge was formed by residues from the C-terminal fragment of the N.BHV domain, i.e. R^{24} and E^{30}, respectively. These salt bridges stabilized the bend structure of the N-end of the protein.

The structurally undefined fragment between helix 1 and helix 2 of UL49.5 had two β-turns of type I in the V26-S29 and E30-Q33 regions. Proline residues participated in the formation of both β-turns. Pro residues could be found very often in the turn structures [60]. Proline is a special residue because it is rigid and pre-bent, thus suites very well for the β-turn format. Furthermore, two or three Pro residues present in an nascent amino acid sequence could act as a specific switch or the hinge [61,62] and thus, might regulate the structure and/or activity of the protein [63–65]. Verweij et al. [55] hypothesized that because the P27 residue was conserved among all the functional UL49.5 inhibitors, it could be responsible for the TAP inhibition. However, their data indicated that the P27 residue did not contribute essentially to the UL49.5-induced inhibition or degradation of TAP. In our structure of UL49.5, the P27 residue was responsible for the turn formation and was located on the surface of the POPC membrane. The other two proline residues, namely P31 and P32, also formed the turn conformation in the E30-Q33 region. They were also located on the surface of the POPC membrane (Fig. 6A) and could be responsible for the appropriate orientation of helix 2 in the membrane. Both the P31 and P32 residues could act as a switch, which allowed the reorientation of the N-terminal domain (ER lumen domain) of the protein. The molecular dynamics of the entire protein, run with the NMR restraints, showed that the N-terminal fragment of the protein adopted a stable helical structure. In turn, the removal of NMR restrains in MD calculations, caused that the helical structure of the N-terminal part was slightly deformed and unfolded. This fragment of the protein maintains a helical character but the helix is probably less stable.

In the transmembrane domain of UL49.5, between helices 2 and 3, characteristic β-turn, stabilized by a hydrogen bond between the M46 carbonyl group and the V49 amide group (Fig. 9S), was observed in the M46-V49 fragment. Side chains of residues M46, V47, A48 and V49 protrude outward the turn. The side chains of these residues possess a strong hydrophobic character and can interact with the hydrophobic

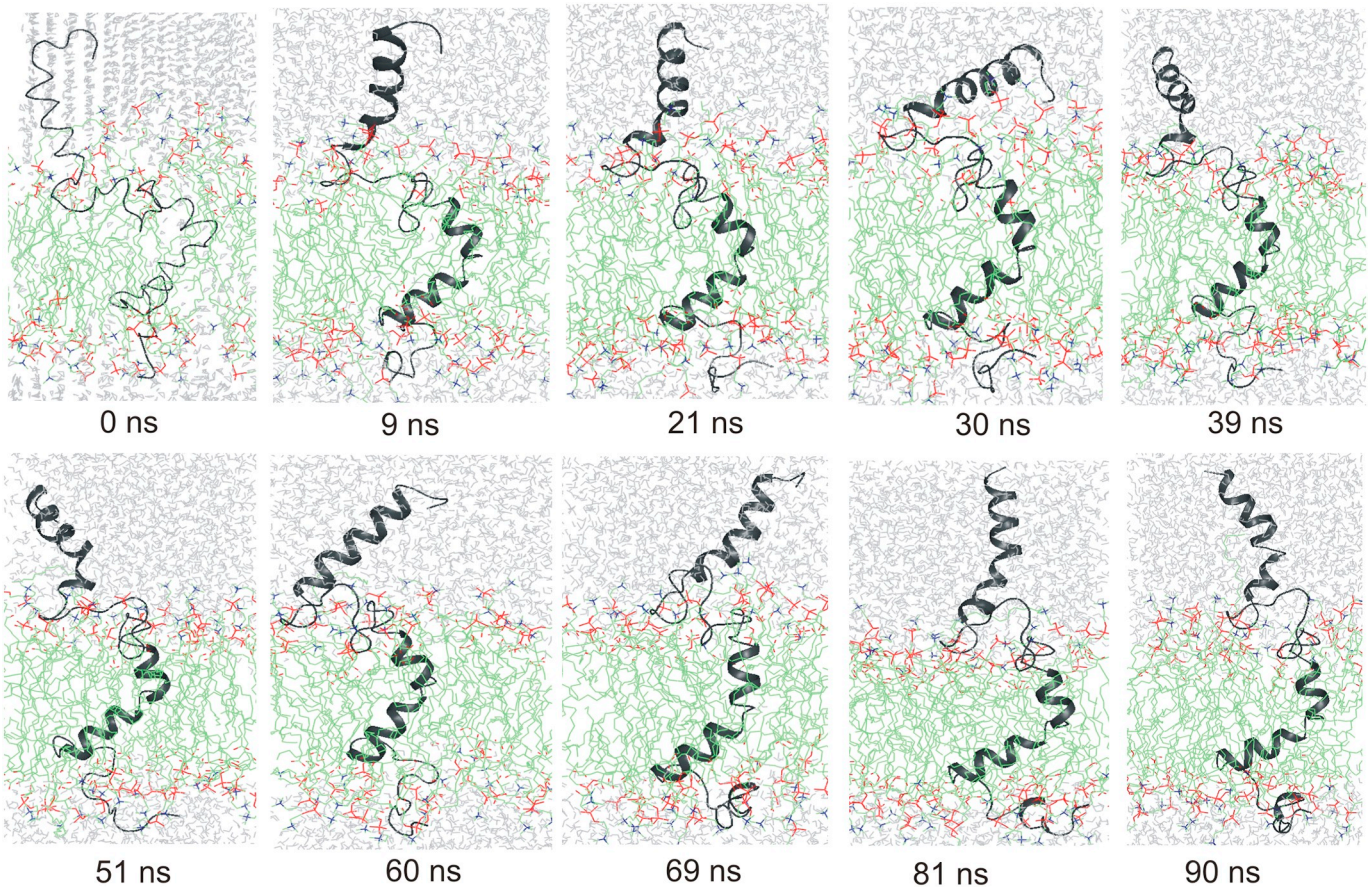

Fig. 4. Snapshots from MD simulations of UL49.5 with NMR (0–40 ns) and no NMR (40–90 ns) restraints.

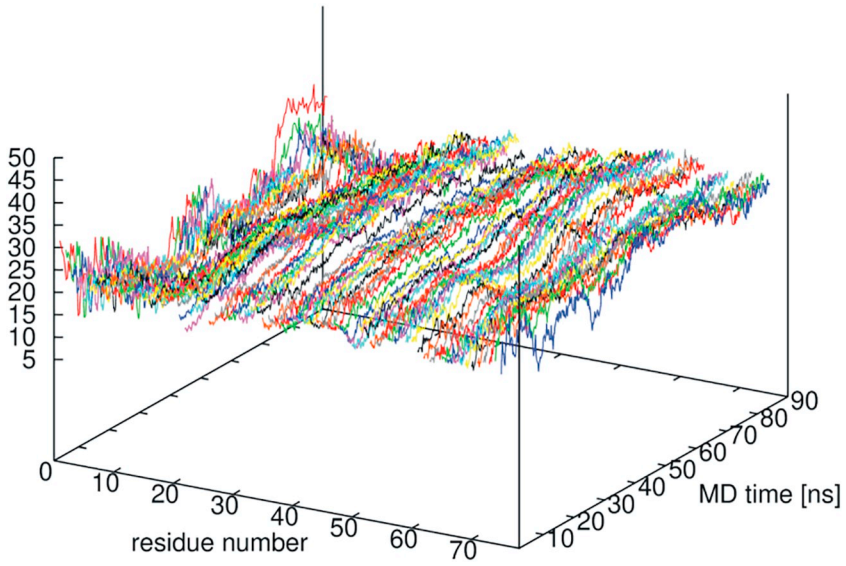

Fig. 5. Movement of Cα atoms of individual amino acid residues of UL49.5 during MD simulation. NMR restraints were kept only between 0 and 40 ns of MD.

part of the POPC membrane (Fig. 6A and C). The hydrophilic parts of these residues were directed inside of the bend (Fig. 9S). Thus, no unfavorable effects between the hydrophilic oxygen atoms and the hydrophobic part of the POPC membrane have been observed. Therefore, the transmembrane domain of UL49.5 created the helix-turn-helix motif. A similar, bent structure in the same region was previously predicted using the I-TASSER program [55]. This characteristic bend, or α-helix break, might be necessary for the appropriate orientation of the protein in the biological membrane or during its interactions with the viral transmembrane glycoprotein M (gM, the UL49.5 partner in the late phase of infection), with another UL49.5 molecule in a homodimer, or with the mammalian TAP complex. The TM helices of other transmembrane proteins can also form helix kinks or bends in their α-helical structures. In most examples, the Pro residues are found in these structures [55].

In the C-terminal cytosolic domain of UL49.5, β-type turn was

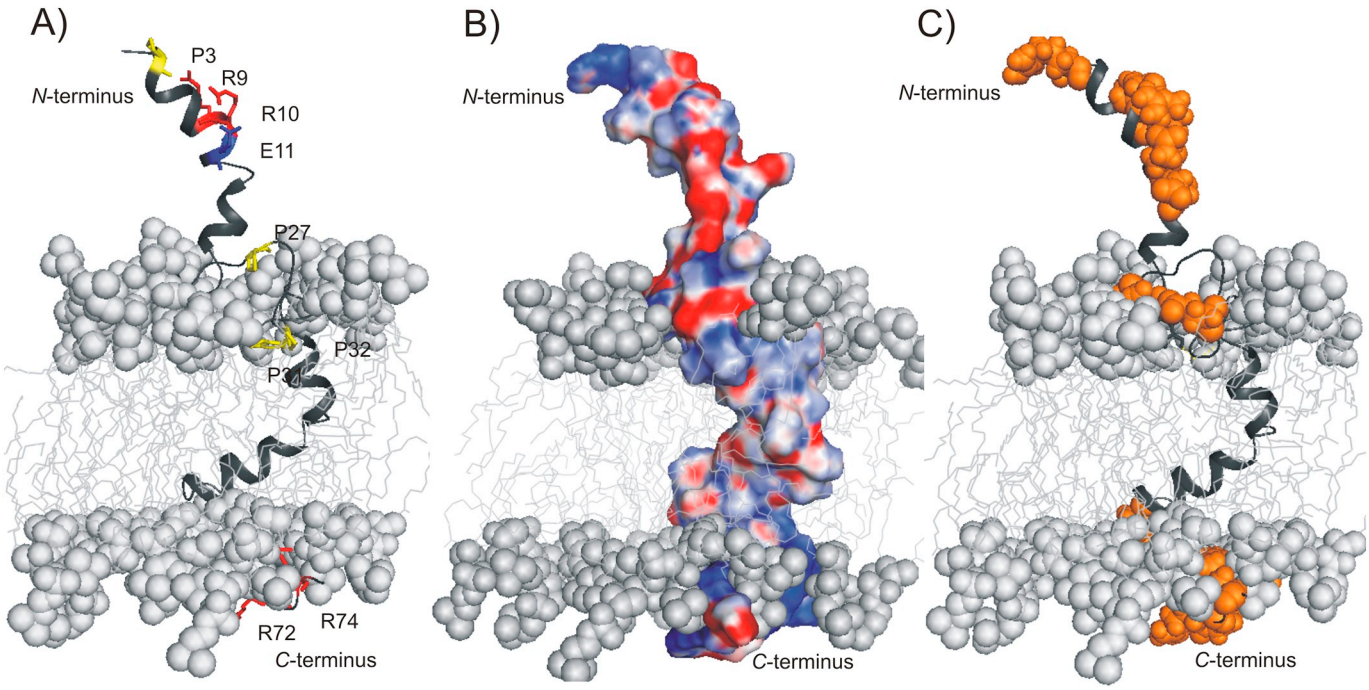

Fig. 6. (A) Structure of UL49.5 obtained after 90 ns of MD simulation in POPC membrane. Protein backbone structure is depicted in ribbon projection. Amino acids are shown in stick projection. (B) Electrostatic potential on van der Waals surface of UL49.5 calculated for the final structure in the POPC membrane. Hydrophobic core of the membrane is shown by light gray lines, and hydrophilic part of the membrane is shown as gray spheres. (C) Surface of charged amino acid residues (Arg, Lys, Asp, and Glu) in UL49.5 protein (orange).

observed in the S64-N67 (SGPN) region. This conformation probably allowed for the appropriate orientation of this region in the POPC membrane. This characteristic bend was stabilized by a salt bridge between the R72 and the E70 residues.

By analyzing the arrangement of UL49.5 in the POPC membrane, we found that the fragment R1-C21 was primarily immersed in water environment (Fig. 6C), whereas the fragment Y22-F58 was mainly buried in the hydrophobic part of the POPC membrane. However, some amino acid residues (P31, P32, A34, L35, V40, T43) preferred to locate in the hydrophilic part of the POPC membrane. The F16 and W17 aromatic amino acid side chains were located on the same α-helix surface and could together potentially interact with gM as was previously suggested by Wei *et al.* [66]. The UL49.5/gM complex was implicated in such processes as the maturation of virions and the control of membrane fusion.

The *C*-terminal fragment of UL49.5 (R59-R72) was immersed in the hydrophilic portion of the membrane. The last three amino acid residues G73-R74-G75 (Fig. 6C) were strongly exposed to the auqeous environment. The *C*-terminal part of UL49.5 was previously implicated in triggering TAP degradation by the proteasome. Viruses frequently utilize the ubiquitin pathway for immune evasion [67], where ubiquitin can be attached not only to the lysine residues but also to the cysteine, serine, and threonine [68]. Therefore, Verweij *et al.* [55] investigated the role of the potential ubiquitination sites of bovine UL49.5 in TAP degradation by using three different mutants of the viral protein. They found that all the mutants had the same effect on TAP stability as the native protein [11]. This implied that the K68, K69, and S71 residues were buried in the biological membrane, making them unaccessible to a (still unknown) E3 ligase that catalyzes UL49.5 Lys or Ser ubiquitination. Our structural analysis is in line with these results indicating low accessibility of potential C-terminal ubiquitination sites. Residues E70–S71 were immersed in the hydrophilic part of the POPC membrane and were not easily accessible to the water molecules and to other cytosolic proteins. Furthermore, the UL49.5 residues R72-G73-R74-G75 were suggested by Verweij *et al.* [55] as a motif responsible for the proteasomal degradation of TAP. The sequence of the RGRG region was strongly sensitive to mutations, especially substitutions of a charged amino acid residue (Arg), which prevented TAP degradation. In particular, Arg at position 72 had a strong effect of this process. Our structural analysis showed that R72 interacted with the hydrophilic part of the POPC membrane, whereas Arg74 was fully accessible to the water molecules. The RGRG motif of UL49.5, extending from the biological membrane, might act as an allosteric proteasome activator in TAP degradation. It might interact with TAP and modify its structure, directing the transporter to ubiquitination pathway and then proteasomal degradation. The RGRG motif with sequences similar to glycine and arginine-rich motifs in proteins interacting with RNA, was efficiently recognized by methyltransferase(s), modifying arginine in numerous proteins [69]. The RG repeats represented targets for type-I protein arginine *N*-methyltransferase. A glycine residue at the *n*-1 position from arginine was highly conserved among the substrates tested for arginine methylation [69–71]. The asymmetrical dimethylation of the arginine residues within these RG repeats could dramatically change protein binding [59]. However, this hypothesis needs to be confirmed by additional experiments.

Looking at the electrostatic potential of the protein, calculated on the surface of the van der Waals complexes (Fig. 6B and C), we concluded that helix 1 was mostly hydrophilic and the most strongly exposed to the water environment. Helix 2 had an amphipathic character, whereas helix 3 was mainly hydrophobic. The electrostatic properties of the individual structural elements of UL49.5 determined the arrangement of these structural elements in the biological POPC membrane.

The final model of the UL49.5 protein was submitted to the Protein Model Database and has been assigned the following ID code: PM0081903.

3.8. Possible structures of UL49.5/TAP/substrate complex

In the first step, UL49.5 was docked to the TAP protein. In this experiment, 30 models of the UL49.5/TAP complexes were generated by the ClusPro program (Fig. 10S) [48,52,50]. Of these, for further analysis only three models (11, 28 and 30) displaying the correct

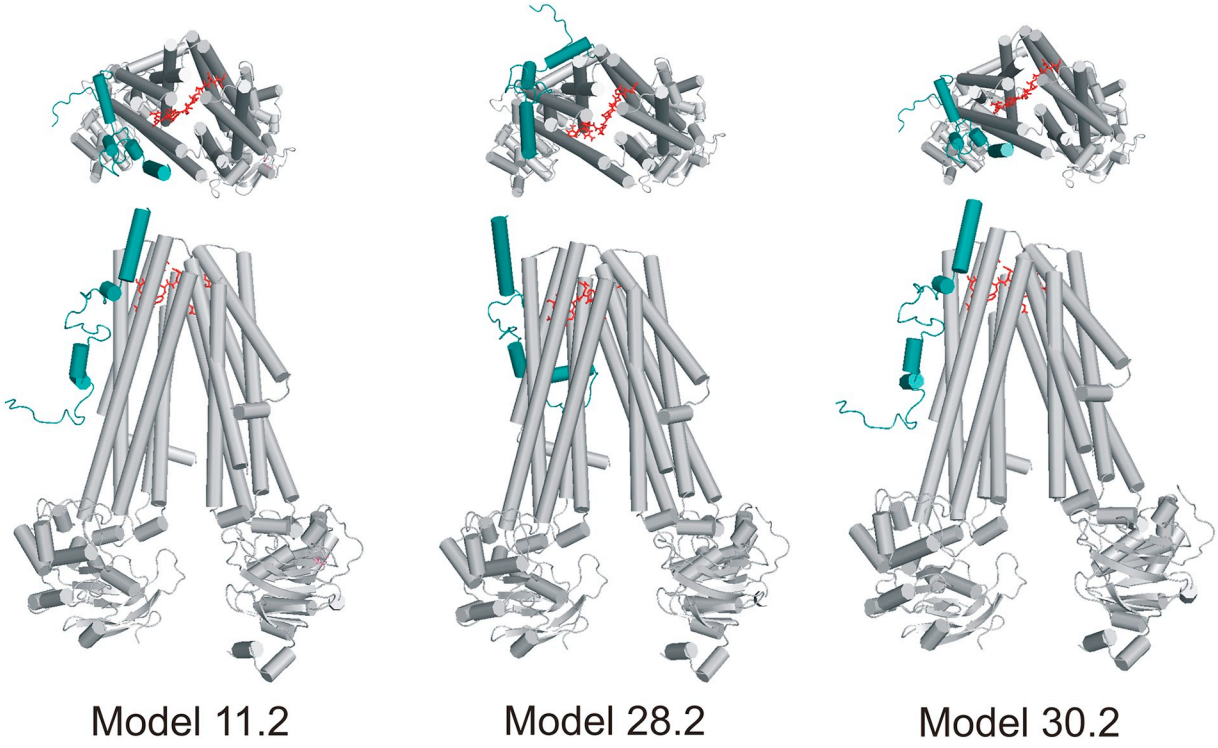

Fig. 7. Structures of UL49.5/TAP/substrate complexes that fulfill the selection criteria. TAP (light gray) and UL49.5 (cyan) are shown in the cartoon projection. Substrate (peptide) is indicated in the stick projection (red). (A) top view, (B) side view of the models.

location and orientation of UL49.5 in the membrane (Fig. 7), and the possible interaction of the *N*-terminal UL49.5 fragment with the TAP protein loop on the ER lumen side, as it was proposed in the literature [12], were selected. In each of the selected models, UL49.5 was bound to TAP at different locations. The UL49.5 luminal domain residues 7–11 were previously found as crucial inhibition of the human TAP and downregulation of MHC I surface expression [6]. Other studies by Wei *et al.* [66] also showed a very important role of the $R^{9}R^{10}E^{11}$ residues from the ER lumen, what was explained by the presence of electrostatic interactions between the two positively charged amino acid residues from UL49.5 and the negatively charged amino acids located in the TAP protein loops from the ER lumen side. In our three models 11, 28 and 30, the RRE motif of UL49.5 could interact with the ER loops of TAP. The most favorable electrostatic interactions were observed in Model 30, where R9 residue interacts with aspartic acid and serine from the ER luminal loop of TAP1.

In addition, in the three selected models, UL49.5 interacted simultaneously with TAP1 and TAP2, which was in agreement with the literature data. The optimal binding of UL49.5 to TAP required both TAP subunits [5], what could be seen in Models 11 and 30, where UL49.5 interacted with the wide surface of TAP. In the case of Model 28, UL49.5 could interact primarily with the TAP protein and only the *C*-terminus of UL49.5 interacts with TAP2. UL49.5 can cause the downregulation of the MHC I surface expression and interact with the TAP complex in the absence of the *N*-terminal domains of TAP1 and TAP2. However, deletion of the *N*-terminal part of TAP2 negatively influenced the binding of UL49.5 and the efficiency of the TAP inhibition. Probably, UL49.5 mainly targets the 6 + 6 TM core of TAP, but requires also the *N*-terminal region of TAP2 for the optimal inhibition of TAP. Presumably this TAP domain could stabilize the TAP complex in a conformation that favors the UL49.5-TAP interaction [11]. In our theoretical models, UL49.5 interacted with the *N*-terminal region of the TAP2 protein and with the loop between TM2 and TM3 of TAP2 only in Models 11 and 30. In Model 28, the interactions of UL49.5 with TAP2 were weak. The analysis of the interactions between the *C*-terminal $R^{72}GRG^{75}$ motif showed the presence of electrostatic interactions between UL49.5 and TAP only in Model 11. The *C*-terminal RGRG motif of UL49.5 might be responsible for the appropriate orientation of UL49.5 in biological membranes, driven by strong electrostatic interactions between the arginine side chains and the lipid heads.

Because UL49.5 interacts with TAP and inhibits peptide (substrate) transport, in the next step, three models of UL49.5/TAP complexes were used to analyze the substrate molecular docking. In this experiment, the peptide substrate (H_2N-R^{1}RYQK5STEL^{9}-$CONH_2$) [5,7] of TAP was docked into each of the three selected models of the UL49.5/TAP complex. Thus, for Models 11, 28, and 30, eight, seven and eleven UL49.5/TAP/substrate complexes were generated, respectively. In total, 26 UL49.5/TAP/substrate complexes were obtained and subsequently analyzed. In all complexes, the substrate interacted almost identically with the upper part of the inward-open TAP conformation and located inside of TAP. In Fig. 7 we show only three examples of UL49.5/TAP/substrate complexes. In these three models, UL49.5 is located on the outside of TAP. The *N*-terminal domain of UL49.5 is located at ER lumen, and the *C*-terminal domain is exposed to the intracellular space. Unfortunately, in all obtained complexes the substrate did not bound to its canonical binding pocket described previously in the literature [12].

In this study, we used the only accessible TAP protein model from the PDB data bank (PDB code: 5u1d) [12]. This structure is shown to adopt the inward-open conformation, which was unlikely to be characteristic of a UL49.5-bound transporter. According to the literature, UL49.5 freezes TAP in a conformation that can bind both the substrate and ATP, but it is unable to translocate the peptide [73]. Although the available TAP structure the most likely does not take the correct arrangement of the transporter bound to UL49.5 into account, it may reveal various possibilities for the interaction with UL49.5. Our results show that Model 11, with an interesting orientation and localization of the P27, P31, and P32 residues of UL49.5, exhibited the most optimal interaction potential with TAP (Fig. 7). These observations are very interesting in light of the previous studies, which suggested that P31 or

P32 were important for the appropriate folding of UL49.5 and for the appropriate interaction of UL49.5 with TAP [55]. The orientation of UL49.5 in the UL49.5/TAP complex and the role of the P27, P31, and P32 amino acids in the interaction with TAP should be investigated in future studies by using molecular biology tools.

4. Conclusions

BHV-1-encoded UL49.5 is a member of the family of varicellovirus-encoded TAP inhibitors. Thus far, other TAP-inhibiting UL49.5 proteins have been found in bovine herpesvirus 5, pseudorabies virus, equine herpesvirus 1 and 4, cervid herpesvirus 1, feline herpesvirus 1, and canine herpesvirus. These proteins efficiently block the peptide transport by TAP, thereby preventing the MHC I-mediated presentation of viral peptides and the subsequent elimination of the infected cells by specific cytotoxic T lymphocytes [11,73]. UL49.5 demonstrates direct interactions with membrane lipids and membrane viral or cellular proteins. In this study, we determined the structure of BHV-1 UL49.5 to find its contribution to the interaction with TAP and to the induced immune evasion. To the best of our knowledge, thus far, no studies on the experimental determination of the structure of UL49.5 have been reported. Knowledge about the 3D structure of this protein can help to explain its interactions and the modulation of TAP during immune inhibition.

As the UL49.5 protein has 75 residues, for our NMR studies, UL49.5 was analyzed as two independent protein fragments. This approach let us record the UL45.9 structure under NMR conditions similar to those occurring naturally in an ongoing infectious process. The first fragment of the protein contained 35 amino acid residues, and the second one contained 40 amino acid residues. A similar approach to the determination of the spatial structure of a membrane protein was used by Mahajan *et al.* [74], who divided the SARS-CoV fusion protein into two fragments to measure the NMR spectra and establish their structures.

Several CD studies using DPC or POPC have suggested that transmembrane proteins derived from pathogenic microorganisms might have a helical intramembrane structure [19]. Our CD data showed that the *N*-terminal (N.BHV) and the transmembrane–cytoplasmic (TMC.BHV) fragments of UL49.5 adopted helical structures induced by the biological membrane environment. The CD spectra of these two fragments in PBS or in water showed a high content of unordered conformation. Similar studies were performed for the *N*-terminal half of the ICP47 protein, another TAP viral inhibitor [75]. This peptide was as active in the inhibition of human TAP as the full-length protein. The CD studies of this peptide showed that the viral inhibitor of TAP appeared to be primarily unstructured in an aqueous solution. However, in the presence of membrane mimetics or lipid membranes, an α-helical structure was formed [75]. In this study, the helical structure of the protein fragments was also confirmed by NMR spectra, which showed the backbone and side-chain NOE effects characteristic of helix structures in the short regions of the investigated peptides. In this paper, the NMR-calculated structure of the N.BHV peptide consisted primarily of a right-handed α-helix in the A7-G20 regions, whereas TMC.BHV consisted primarily of a right-handed α-helix in the V40-Nle46 and V49-F58 regions. The regions forming helical structures in the presence of DPC micelles were almost similar to those predicted for the UL45.9 protein in the POPC membrane environment. The final structure of UL49.5 in the POPC membrane consisted of three α-helical regions. Helix 1 (D2-G20) was located at the *N*-terminal fragment region (ER lumen domain), helix 2 (V40-M46) and helix 3 (V49-M61) in the middle transmembrane region of UL49.5.

This UL49.5 structure remained significantly different from that proposed using a theoretical approach [15]. Similarly, our data showed the helices inside the cellular membrane (Fig. 6A) [13]. According to our results, the ER luminal domain consisting of 1–21 residues was exposed to the aqueous medium and the rest of the domain was immersed in the charged or hydrophobic portion of the POPC membrane. However, in the theoretical structure of UL49.5 [13], the *N*-terminal domain (1–40) is fully exposed to the water environment. The predicted 3D structure of UL49.5 from BHV-1 revealed a characteristic bend in the ER luminal domain that was facilitated by P27, whereas according to our results, two β-turns were observed in this domain in the regions V26-P27-L28-S29 and E30-P31-P32-Q33. Both β-turns engaged the Pro residues, which might be important for the specific folding of UL49.5 and the interaction between UL49.5 and TAP and, consequently, the inhibition of peptide transport. Remarkably, P30/P32 were conserved among the TAP-inhibiting UL49.5 homologs. The substitution of these residues by alanine influenced the TAP activity, implying that the structure facilitated by the Pro residues was crucial for the BHV-1 UL49.5 function [unpublished data].

Our structure had two transmembrane helices whose continuity was interrupted by β-turn in the M46-V49 region. Helices 2 and 3 of the transmembrane domain were stacked at an angle of approximately 110° and together with the turn structure formed the helix-turn-helix motif. In the theoretically predicted structure, the transmembrane domain also formed two helical regions connected by a shorter unordered region; the helices were arranged at an angle of approximately 110° to each other. In our structure, helix 3 had the amphipathic character and could partly interact with the head groups of the POPC membrane. Similar localization in the biological membrane and similar structure, also containing the helix-turn-helix motif, with interaction of a short helix interaction with the polar groups of lipids was found in the Ebola virus envelope protein [53]. This protein also had an *N*-terminal domain exposed to the outside of the membrane.

In this study, the *C*-terminal domain of UL49.5 was primarily immersed in the charged portion of the membrane and only the three last amino acid residues were strongly exposed to the solvent, whereas in the predicted structure. The cytosolic domain (R59–G75 fragment) was fully exposed to the water molecules. In both structures (this study and predicted), the *C*-terminus is unstructured with the characteristic bend facilitated by P66. Of note that in the structure we obtained, the RGRG fragment of the cytosolic *C*-terminal domain protruded from the membrane and thus, could potentially interact with other proteins and modulate their functions.

In this study, we also obtained three possible structures of the UL49.5/TAP complexes, UL49.5 in these complexes was located on the outside of TAP, with the most probable structure represented by very similar Models 11 and 30. This is the first known structure of the UL49.5/TAP protein complex. Because of the lack of experimental evidence for the specific binding site of the UL49.5 to TAP, which of the proposed complexes is most closely related to the real structure is unknown. Furthermore, experimental research related to the mutagenesis of the TAP protein is highly warranted.

Transparency document

The Transparency document associated with this article can be found, in online version.

Acknowledgments

This work was supported by the following grants: POMOST/2010/2-7 from Foundation for Polish Science and UMO-2014/14/E/NZ6/00164 from Polish National Science Center (Andrea Lipińska). The authors would like to thank Dr. Jue Chen, Howard Hughes Medical Institute, The Rockefeller University, USA for sharing the 5u1d ICP47-TAP structure before it was published.

Appendix A. Supplementary data

Supplementary data to this article can be found online at https://doi.org/10.1016/j.bbamem.2019.02.005.

References

[1] A.J. Davison, Herpesvirus systematics, Vet. Microbiol. 143 (2010) 52–69.
[2] L. Turin, S. Russo, G. Poli, BHV-1: new molecular approaches to control a common and widespread infection, Mol. Med. 5 (1999) 261–284.
[3] D. Horst, M.C. Verweij, A.J. Davison, M.E. Ressing, E.J.H.J. Wiertz, Viral evasion of T cell immunity: ancient mechanisms offering new applications, Curr. Opin. Immunol. 23 (2011) 96–103, https://doi.org/10.1016/j.coi.2010.11.005.
[4] A.D. Lipińska, D. Koppers-Lalic, M. Rychłowski, P. Admiraal, F.A.M. Rijsewijk, K. Bieńkowska-Szewczyk, E.J.H.J. Wiertz, Bovine herpesvirus 1 UL49.5 protein inhibits the transporter associated with antigen processing despite complex formation with glycoprotein M, J. Virol. 80 (2006) 5822–5832, https://doi.org/10.1128/JVI.02707-05.
[5] D. Koppers-Lalic, E.A.J. Reits, M.E. Ressing, A.D. Lipinska, R. Abele, J. Koch, M. Marcondes Rezende, P. Admiraal, D. van Leeuwen, K. Bienkowska-Szewczyk, T.C. Mettenleiter, F.A.M. Rijsewijk, R. Tampé, J. Neefjes, E.J.H.J. Wiertz, Varicelloviruses avoid T cell recognition by UL49.5-mediated inactivation of the transporter associated with antigen processing, Proc. Natl. Acad. Sci. U. S. A. 102 (2005) 5144–5149, https://doi.org/10.1073/pnas.0501463102.
[6] S. Loch, F. Klauschies, C. Schölz, M.C. Verweij, E.J.H.J. Wiertz, J. Koch, R. Tampé, Signaling of a varicelloviral factor across the endoplasmic reticulum membrane induces destruction of the peptide-loading complex and immune evasion, J. Biol. Chem. 283 (2008) 13428–13436, https://doi.org/10.1074/jbc.M800226200.
[7] V. Corradi, G. Singh, D.P. Tieleman, The human transporter associated with antigen processing: molecular models to describe peptide binding competent states, J. Biol. Chem. 287 (2012) 28099–28111, https://doi.org/10.1074/jbc.M112.381251.
[8] J. Koch, R. Guntrum, S. Heintke, C. Kyritsis, R. Tampé, Functional dissection of the transmembrane domains of the transporter associated with antigen processing (TAP), J. Biol. Chem. 279 (2004) 10142–10147, https://doi.org/10.1074/jbc.M312816200.
[9] N. Grossmann, A.S. Vakkasoglu, S. Hulpke, R. Abele, R. Gaudet, R. Tampé, Mechanistic determinants of the directionality and energetics of active export by a heterodimeric ABC transporter, Nat. Commun. 5 (2014) 5419, , https://doi.org/10.1038/ncomms6419.
[10] J. Geng, S. Sivaramakrishnan, Analyses of conformational states of the transporter associated with antigen processing (TAP) protein in a native cellular membrane environment, J. Biol. Chem. 288 (2013) 37039–37047.
[11] M.C. Verweij, D. Koppers-Lalic, S. Loch, F. Klauschies, H. de la Salle, E. Quinten, P.J. Lehner, A. Mulder, M.R. Knittler, R. Tampé, J. Koch, M.E. Ressing, E.J.H.J. Wiertz, The varicellovirus UL49.5 protein blocks the transporter associated with antigen processing (TAP) by inhibiting essential conformational transitions in the 6+6 transmembrane TAP core complex, J. Immunol. 181 (2008) 4894–4907, https://doi.org/10.4049/jimmunol.181.7.4894.
[12] M.L. Oldham, J. Chen, N. Grigorieff, Structure of the transporter associated with antigen processing trapped by herpes simplex virus, Elife. (2016) 255–278, https://doi.org/10.7554/eLife.21829.
[13] M.C. Verweij, D. Horst, B.D. Griffin, R.D. Luteijn, A.J. Davison, M.E. Ressing, E.J.H.J. Wiertz, Viral inhibition of the transporter associated with antigen processing (TAP): a striking example of functional convergent evolution, PLoS Pathog. 11 (2015) 1–20, https://doi.org/10.1371/journal.ppat.1004743.
[15] J. Radoicic, G.J. Lu, S.J. Opella, NMR structures of membrane proteins in phospholipid bilayers, Q. Rev. Biophys. 47 (2014) 249–283, https://doi.org/10.1017/S0033583514000080.
[16] D.A. Kallick, M.R. Tessmer, C.R. Watts, C.Y. Li, The use of dodecylphosphocholine micelles in solution NMR, J. Magn. Reson. B 109 (1995) 60–65, https://doi.org/10.1006/jmrb.1995.1146.
[17] K. Murzyn, T. Róg, G. Jezierski, Y. Takaoka, M. Pasenkiewicz-Gierula, Effects of phospholipid unsaturation on the membrane/water interface: a molecular simulation study, Biophys. J. 81 (2001) 170–183.
[18] M. Pasenkiewicz-Gierula, T. Róg, K. Kitamura, A. Kusumi, Cholesterol effects on the phosphatidylcholine bilayer polar region: a molecular simulation study, Biophys. J. 78 (2000) 1376–1389, https://doi.org/10.1016/S0006-3495(00)76691-4.
[19] D.E. Warschawski, A.A. Arnold, M. Beaugrand, A. Gravel, É. Chartrand, I. Marcotte, Choosing membrane mimetics for NMR structural studies of transmembrane proteins, Biochim. Biophys. Acta Biomembr. 1808 (2011) 1957–1974, https://doi.org/10.1016/J.BBAMEM.2011.03.016.
[20] G.B. Fields, R.L. Noble, Solid phase peptide synthesis utilizing 9-fluorenylmethoxycarbonyl amino acids, Int. J. Pept. Protein Res. 35 (1990) 161–214.
[21] E. Atherton, R.C. Sheppard, Solid Phase Peptide Synthesis: A Practical Approach, Oxford Univ. Press, Oxford, 1989.
[22] N.J. Greenfield, Using circular dichroism spectra to estimate protein secondary structure, Nat. Protoc. 1 (2006) 2876–2890, https://doi.org/10.1038/nprot.2006.202.
[23] T. Rao, G. Ruiz-Gómez, T.A. Hill, H.N. Hoang, Truncated and helix-constrained peptides with high affinity and specificity for the cFos coiled-coil of AP-1, PLoS One 8 (2013) e59415.
[24] G. Manzo, M. Carboni, A.C. Rinaldi, M. Casu, M.A. Scorciapino, Characterization of sodium dodecylsulphate and dodecylphosphocholine mixed micelles through NMR and dynamic light scattering, Magn. Reson. Chem. 51 (2013) 176–183, https://doi.org/10.1002/mrc.3930.
[25] K. Wüthrich, NMR of Proteins and Nucleic Acids, Wiley, 1986.
[26] M. Rance, O.W. Sorenso, G. Bodenhausen, G. Wagner, R.R. Ernst, Improved spectral resoltion in cosy 1H NMR spectra proteins via double quantum filtering, Biochem. Biophys. Res. Commun. 117 (1983) 479–485.
[27] A. Bax, R. Freeman, Enhanced NMR resolution by restricting the effective sample volume, J. Magn. Reson. 37 (1980) 177–181, https://doi.org/10.1016/0022-2364(80)90104-3.
[28] A. Kumar, R.R. Ernst, K. Wüthrich, A two-dimensional nuclear Overhauser enhancement (2D NOE) experiment for the elucidation proton-proton cross relaxation networks in biological macromolecules, Biochem. Biophys. Res. Commun. 95 (1980) 1–10.
[29] A. Bax, D.G. Davis, Practical aspects of two-dimensional transverse NOE spectroscopy, J. Magn. Reson. 63 (1985) 207–213, https://doi.org/10.1016/0022-2364(85)90171-4.
[30] C. Emetarom, T.-L. Hwang, G. Mackin, A.J. Shaka, Isotope editing of NMR spectra. Excitation sculpting using BIRD pulses, J. Magn. Reson. (1995) 137–140.
[31] D.S. Wishart, C.G. Bigam, J. Yao, F. Abildgaard, H.J. Dyson, E. Oldfield, J.L. Markley, B.D. Sykes, 1H, 13C and 15N chemical shift referencing in biomolecular NMR, J. Biomol. NMR 6 (1995) 135–140.
[32] M. Nilsson, A.M. Gil, I. Delgadillo, G.A. Morris, Improving pulse sequences for 3D diffusion-ordered NMR spectroscopy: 2DJ-IDOSY, Anal. Chem. 76 (2004) 5418–5422.
[33] F. Delaglio, S. Grzesiek, G.W. Vuister, G. Zhu, J. Pfeifer, A. Bax, NMRPipe: a multidimensional spectral processing system based on UNIX pipes, J. Biomol. NMR 6 (1995) 277–293.
[34] T.D. Goddard, D.G. Kneller, SPARKY 3, University of California, San Francisco (2001).
[35] P. Güntert, L. Buchner, Combined automated NOE assignment and structure calculation with CYANA, J. Biomol. NMR 62 (2015) 453–471, https://doi.org/10.1007/s10858-015-9924-9.
[36] D.P. Tieleman, D. van der Spoel, H.J.C. Berendsen, Molecular dynamics simulations of dodecylphosphocholine micelles at three different aggregate sizes: micellar structure and chain relaxation, J. Phys. Chem. B 104 (2000) 6380–6388, https://doi.org/10.1021/jp001268f.
[37] E.A. Lubecka, E. Sikorska, D. Sobolewski, A. Prahl, J. Slaninov, J. Ciarkowski, Arginine-, d-arginine-vasopressin, and their inverso analogues in micellar and liposomic models of cell membrane: CD, NMR, and molecular dynamics studies, Eur. Biophys. J. 44 (2015) 727–743, https://doi.org/10.1007/s00249-015-1071-4.
[38] E. Sikorska, D. Wyrzykowski, K. Szutkowski, K. Greber, E.A. Lubecka, I. Zhukov, Thermodynamics, size, and dynamics of zwitterionic dodecylphosphocholine and anionic sodium dodecyl sulfate mixed micelles, J. Therm. Anal. Calorim. 123 (2016) 511–523, https://doi.org/10.1007/s10973-015-4918-0.
[39] D.A. Case, T.A. Darden, C.L. Simmerling, T.E. Cheatham 3rd, K.M. Merz, Amber11 user's manual, AMBER (2011) 1–308.
[40] D.A. Case, J.T. Berryman, R.M. Betz, D.S. Cerutti, T.E. Cheatham 3rd, T.A. Darden, R.E. Duke, T.J. Giese, H. Gohlke, A.W. Goetz, N. Homeyer, S. Izadi, P. Janowski, J. Kaus, A. Kovalenko, T.S. Lee, S. LeGrand, P. Li, T. Luchko, R. Luo, B. Madej, AMBER, (2015).
[41] W.K. Koradi, M. Billeter, MOLMOL: a program for display and analysis of macromolecular structures, J. Mol. Graph. 14 (1996) 52–55.
[42] W.L. DeLano, The PyMOL Molecular Graphics System, Version 1.5.0.4, Schrödinger, LLC, 2002.
[43] M.W. Schmidt, K.K. Baldridge, J.A. Boatz, S.T. Elbert, M.S. Gordon, J.H. Jensen, N. Matsunaga, K.A. Nguyen, S. Su, T.L. Windus, M. Dupuis, General atomic and molecular electronic structure system, J. Comput. Chem. 14 (1993) 1347–1363.
[44] C.I. Bayly, P. Cieplak, W.D. Cornell, P.A. Kollman, A well-behaved electrostatic potential based method using charge restraints for deriving atomic charges: the RESP model, J. Phys. 97 (1993) 10269–10280, https://doi.org/10.1021/j100142a004.
[45] I.W. Davis, A. Leaver-Fay, V.B. Chen, J.N. Block, G.J. Kapral, X. Wang, L.W. Murray, W.B. Arendall, J. Snoeyink, J.S. Richardson, D.C. Richardson, MolProbity: all-atom contacts and structure validation for proteins and nucleic acids, Nucleic Acids Res. 35 (2007) 375–383, https://doi.org/10.1093/nar/gkm216.
[46] S. Costantini, G. Colonna, A.M. Facchiano, Bioinformation ESBRI: a web server for evaluating salt bridges in proteins, Bioinformation. 3 (2008) 137–138, https://doi.org/10.6026/97320630003137.
[47] M. Pasenkiewicz-Gierula, K. Murzyn, T. Róg, C. Czaplewski, Molecular dynamics simulation studies of lipid bilayer systems, Acta Biochim. Pol. 47 (2000) 601–611.
[48] T. Williams, C. Kelley, Gnuplot 4.5: An Interactive plotting Program, http://gnuplot.info, (2011).
[49] D. Kozakov, D. Beglov, T. Bohnuud, S. Mottarella, B. Xia, D.R. Hall, S. Vajda, How good is automated protein docking? Proteins 81 (2013) 2159–2166.
[50] D. Kozakov, D.R. Hall, B. Xia, K.A. Porter, D. Padhorny, C. Yueh, The ClusPro web server for protein–protein docking, Nat. Protoc. 12 (2017) 255–278, https://doi.org/10.1038/nprot.2016.169.
[52] S.R. Comeau, D.W. Gatchell, S. Vajda, C.J. Camacho, ClusPro: an automated docking and discrimination method for the prediction of protein complexes, Bioinformatics. 20 (2004) 45–50, https://doi.org/10.1093/bioinformatics/btg371.
[53] J. Lee, D.A. Nyenhuis, E.A. Nelson, D.S. Cafiso, J.M. White, L.K. Tamm, Structure of the Ebola virus envelope protein MPER/TM domain and its interaction with the fusion loop explains their fusion activity, Proc. Natl. Acad. Sci. 201708052 (2017), https://doi.org/10.1073/pnas.1708052114.
[54] J. Dev, D. Park, Q. Fu, J. Chen, H.J. Ha, F. Ghantous, T. Herrmann, W. Chang, Z. Liu, G. Frey, M.S. Seaman, B. Chen, J.J. Chou, Structural basis for membrane anchoring of HIV-1 envelope spike, Science 353 (80) (2016) 172–175, https://doi.org/10.1126/science.aaf7066.
[55] M.C. Verweij, A.D. Lipińska, D. Koppers-Lalic, E. Quinten, J. Funke, H.C. van Leeuwen, K. Bieńkowska-Szewczyk, J. Koch, M.E. Ressing, E.J.H.J. Wiertz, Structural and functional analysis of the TAP-inhibiting UL49.5 proteins of varicelloviruses, Mol. Immunol. 48 (2011) 2038–2051, https://doi.org/10.1016/j.molimm.2011.06.438.

[56] L. Moroder, Isosteric replacement of sulfur with other chalcogens in peptides and proteins, J. Pept. Sci. 11 (2005) 187–214, https://doi.org/10.1002/psc.654.
[57] L. Moroder, W. Göhring, R. Nyfeler, R. Scharf, P. Thamm, Zur Synthese von Human-Little-Gastrin-I und dessen Leucin-15-, Norleucin-15- und Methoxinin-15-Analoga, Physiol. Chem. 364 (1983) 157–171.
[58] A.M. Gilles, P. Marliere, T. Rose, R. Sarfati, R. Longin, A. Meier, S. Fermandjian, M. Monnot, G.N. Cohen, O. Barzu, Conservative replacement of methionine by norleucine in *Escherichia coli* adenylate kinase, J. Biol. Chem. 263 (1988) 8204–8209.
[59] H. Wei, J. He, D.B. Paulsen, S.I. Chowdhury, Bovine herpesvirus type 1 (BHV-1) mutant lacking U L49.5 luminal domain residues 30-32 and cytoplasmic tail residues 80-96 induces more rapid onset of virus neutralizing antibody and cellular immune responses in calves than the wild-type strain Cooper, Vet. Immunol. Immunopathol. 147 (2012) 223–229, https://doi.org/10.1016/j.vetimm.2012.04.015.
[60] P. Argos, J. Palau, Amino acid distribution in protein secondary structures, Int. J. Pept. Protein Res. 19 (1982) 380–393.
[61] M. Bergdol, M. Remy, C. Cagnon, J. Masson, Proline dependent oligomerization with arm exchange, Structure. 5 (1997) 391–401.
[62] S. Jenko Kokalj, G. Guncar, I. Stern, G. Morgan, S. Rabzelj, M. Kenig, R.A. Staniforth, J.P. Waltho, E. Zerovnik, Essential role of proline isomerization in stefin B tetramer formation, J. Mol. Biol. 5 (2007) 1569–1579.
[63] G. Smaldone, M. Vigorita, A. Ruggiero, N. Balasco, J.D. Dattelbaum, S. D'Auria, P. Del Vecchio, G. Graziano, L. Vitagliano, Proline 235 plays a key role in the regulation of the oligomeric states of Thermotoga maritima arginine binding protein, Biochim. Biophys. Acta, Proteins Proteomics 1864 (2016) 814–824, https://doi.org/10.1016/J.BBAPAP.2016.04.006.
[64] P. Rezácová, D. Borek, S.F. Moy, A. Joachimiak, Z. Otwinowski, Crystal structure and putative function of small Toprim domain-containing protein from Bacillus stearothermophilus, Proteins. 70 (2008) 311–319, https://doi.org/10.1002/prot.
[65] M. Dujardin, V. Madan, R. Montserret, P. Ahuja, I. Huvent, H. Launay, A. Leroy, R. Bartenschlager, F. Penin, G. Lippens, X. Hanoulle, A proline-tryptophan turn in the intrinsically disordered domain 2 of NS5A protein is essential for hepatitis C virus RNA replication, J. Biol. Chem. 290 (2015) 19104–19120, https://doi.org/10.1074/jbc.M115.644419.
[66] H. Wei, Y. Wang, S.I. Chowdhury, Bovine herpesvirus type 1 (BHV-1) UL49.5 luminal domain residues 30 to 32 are critical for MHC-I down-regulation in virus-infected cells, PLoS One 6 (2011), https://doi.org/10.1371/journal.pone.0025742.
[67] F. Randow, P.J. Lehner, Viral avoidance and exploitation of the ubiquitin system, Nat. Cell Biol. (2009) 527–534.
[68] X. Wang, R.A. Herr, W.J. Chua, L. Lybarger, E.J.H.J. Wiertz, T.H. Hansen, Ubiquitination of serine, threonine, or lysine residues on the cytoplasmic tail can induce ERAD of MHC-I by viral E3 ligase mK3, J. Cell Biol. 177 (2007) 613–624, https://doi.org/10.1083/jcb.200611063.
[69] J. Najbauer, B.A. Johnson, A.L. Young, D.W. Aswad, Peptides with sequences similar to glycine, arginine-rich motifs in proteins interacting with RNA are efficiently recognized by methyltransferase(s) modifying arginine in numerous proteins, J. Biol. Chem. 268 (1993) 10501–10509.
[70] K.S. Ghosh, S.K. Syed, S. Jung, W.K. Paik, Substrate specificity for myelin basic protein-specific protein methylase, I, Biochim. Biophys. Acta 1039 (1990) 142–148.
[71] S. Kim, B.M. Merrill, R. Rajpurohit, A. Kumar, K.L. Stone, V.V. Papov, J.M. Schneiders, W. Szer, S.H. Wilson, W.K. Paik, Identification of N(G)-methylarginine residues in human heterogeneous RNP protein A1: Phe/Gly-Gly-Gly-Arg-Gly-Gly-Gly/Phe is a preferred recognition motif, Biochemistry. 36 (1997) 5185–5192.
[73] M.C. Verweij, A.D. Lipinska, D. Koppers-Lalic, W.F. van Leeuwen, J.I. Cohen, P.R. Kinchington, I. Messaoudi, K. Bienkowska-Szewczyk, M.E. Ressing, F.A.M. Rijsewijk, E.J.H.J. Wiertz, The capacity of UL49.5 proteins to inhibit TAP is widely distributed among members of the genus Varicellovirus, J. Virol. 85 (2011) 2351–2363, https://doi.org/10.1128/JVI.01621-10.
[74] M. Mahajan, D. Chatterjee, K. Bhuvaneswari, S. Pillay, NMR structure and localization of a large fragment of the SARS-CoV fusion protein: implications in viral cell fusion, Biochim. Biophys. Acta 17 (2017) 30312–30317.
[75] D. Beinert, L. Neumann, S. Uebel, Structure of the viral TAP-inhibitor ICP47 induced by membrane association, Biochemistry. 36 (1997) 4694–4700.